2016-10

Impacts of port development on estuarine morphodynamics: Ribadeo (Spain)

Prumm, M

10.1016/j.ocecoaman.2016.05.003
Ocean & Coastal Management
Elsevier BV

IMPACTS OF PORT DEVELOPMENT ON ESTUARINE MORPHODYNAMICS: RIBADEO (SPAIN)

MATTHEW PRUMM[1], GREGORIO IGLESIAS[2]

1 Cardno, Australia, matthew.prumm@cardno.com.au
2 Plymouth University, UK, gregorio.iglesias@plymouth.ac.uk

CORRESPONDING AUTHOR:

Prof Gregorio Iglesias

Plymouth University

gregorio.iglesias@plymouth.ac.uk

ABSTRACT

Port developments in estuaries can significantly affect the estuarine dynamics, causing hydrodynamic changes that can in turn affect the sediment transport patterns. Understanding these impacts is crucial given the socioeconomic relevance of estuaries and their high sensitivity as the complex natural systems that they are. The objective of this work is to investigate the impact of port expansion on estuarine dynamics through a case study. Process-based models are implemented to investigate the morphodynamic response of the estuary to the expansion of the Port of Ribadeo. The models simulate the hydrodynamics and sediment transport of the estuary with and without the port development. In total, 12 scenarios are considered: pre- and post-port development cases; morphological times of 1, 2 and 4 years; and two tidal energy situations (equinoctial and solstitial tides, i.e. high and low energy, respectively). The models are forced with the tide (prescribed through the nine major constituents) and river inflow, and the significant variation in sediment size over the estuary is accounted for. Excellent agreement ($R > 0.95$) is achieved between computed and observed water levels and flow velocities. Having validated the model, pre- and post-development cases are compared to determine the effects of the port expansion on estuarine dynamics. We find that the expansion has led to a deepening and straightening of the primary channel of the estuary, with a marked increase in sedimentation either side. This has negative implications for the operation of the Port of Figueras, and in particular for its shipyard, on the other side of the estuary (opposite the Port of Ribadeo) – which proves the potential of port expansions for non-localised impacts on estuarine activities.

KEYWORDS

port management; coastal management; morphodynamics; estuary; Ribadeo

FIGURE SIZE

Figure Size: (Single, 1.5, Full)

Fig 1	Full
Fig 2	Full
Fig 3	Single
Fig 4	1.5
Fig 5	Full
Fig 6	Full
Fig 7	Full
Fig 8	Full
Fig 9	Full
Fig 10	Full
Fig 11	Full
Fig 12	Full
Fig 13	1.5
Fig 14	Full
Fig 15	Full
Fig 16	Full

1. INTRODUCTION

Many ports worldwide are located in estuaries (European Commission, 2011):Lisbon, Rotterdam, Ferrol, Vigo, Newport, etc. Their expansion in an era of growing shipping traffic can have a significant impact on estuarine dynamics, which may be problematic due to the sensitivity of these complex environments. Shifts in estuarine hydrodynamics can trigger feedback mechanisms which may alter the morphology of the estuary. The objective of this paper is to investigate the impacts of port expansion on estuarine morphodynamics through a case study: Ria de Ribadeo, an estuary of the ria type, in particular a Cantabrian ria (Iglesias and Carballo, 2011) in Galicia, NW Spain. Galician rias present complex circulation patterns (Carballo et al., 2009) and have been shown to be sensitive to anthropogenic influence (Ramos et al., 2014b, 2013; Sánchez et al., 2014).

The need to fully comprehend these anthropogenic effects on estuarine environments is increasing, as population and shipping trade grow (Maren et al., 2015) and infrastructure encroaches on estuarine areas. The shipping industry is undergoing major changes as a consequence of the expansion of international trade and shipping traffic, increases in ship sizes and evolution of cargo handling methods (Saz-Salazar et al., 2012). In the case of Spain, the growth of the port system over the past two decades has also been fuelled by a political decentralisation of port management, allowing greater private initiative (Castillo-Manzano et al., 2013). These factors contribute to port development projects as the existing infrastructure becomes insufficient or inadequate, and these developments can provide immense value to the local and national economies (Zhao and Bin, 2005).

Port developments typically include engineered obstacles to the natural flow in the form of breakwaters, quays and jettys, and the environmental responses to these obstacles are necessitate consideration beyond economic viability, of biological and sociological factors (Kamphuis, 2006). Morphological variations are among the most perceptible of these responses, potentially causing undesired infilling of navigation channels, erosion around pipelines and structural foundations or sedimentation in and around ports and harbours. The environmental pressure induced by continuing increases in urban development and economic activities in coastal areas is well documented, with researchers noting improvements in management policies may be required to control these effects (e.g. Taveira Pinto, 2004; Veloso-Gomes and Taveira-Pinto, 2003). Port management and coastal morphodynamics are both fields of active research, recently branching into sub-topics such as implementation of wave energy devices in port design and coastal defence schemes (Abanades et al., 2014a, 2014b, 2015; Buccino et al., 2015; Vicinanza et al., 2014).

Retrospective analyses of coastal and estuarine morphology are made possible with tools such as aerial photography, Geographical Information Systems (GIS) and bathymetric surveys (e.g. Monge-Ganuzas et al., 2013; Wu et al., 2011). However, the prediction of morphological responses is far more complicated. Statistical models based on observational data have been implemented to form multi-criteria predictions of coastal environments incorporating marine geology among other elements such as water quality and marine ecosystems (e.g. Kim and Park, 2015), while process-based numerical models have been successfully used for analyses of coastal processes and shoreline evolution (e.g. Abanades et al., 2014c; López-Ruiz et al., 2012; Ortega-Sánchez et al., 2003). Technological advancements have facilitated the use of process-based numerical models for long-term (inter-decadal) morphodynamic investigations, calibrated and validated via historical analyses (e.g. Dastgheib et al., 2008; Dissanayake et al., 2009; Liu, 2013; van der Wegen, 2010). Despite the increasing presence of morphological studies in literature, process-based models aimed at determining consequences of direct anthropological modification are relatively sparse, examples include Dissanayake et al. (2012b), Kuang et al. (2013) and Maren et al. (2015).

Effective coastal and estuarine management requires an understanding of the broad environmental impacts associated with coastline modifications, and consideration of the potential for negative consequences to various stakeholder operations. Furthermore, improved understanding of morphodynamic responses to these developments may allow advantageous design. For example, this knowledge could be used to design future defences, ports and harbours in such a way as to reduce both undesirable morphological effects within the estuary and local dredging requirements, often a high on-going expense.

Although sparse, there exist some investigations of direct anthropogenic modifications to estuarine morphodynamics. Past technological limitations did not deter the scientific community from attempting to simulate these modifications in 1D (Spearman et al., 1998). More recently, process-based modelling has been applied in 2D to determine long-term responses to large anthropogenic obstacles in the Wadden Sea (Dissanayake et al., 2012b). The accuracy of process-based models is increasing, with more effective parameterisations of natural processes and enhanced computational power. There is now no reason that medium to long-term morphodynamic responses to various estuarine structures cannot be investigated in other locations.

1.1. STUDY AREA

The Ribadeo estuary, ‘Ria de Ribadeo’ or ‘Ria del Eo’ in the vernacular, is a ria in Galicia, NW Spain. Rias are a specific type of estuary, defined as an inundated fluvial valley, where the coastline

and bathymetry bear similarities to the geometry of the river valley from which they originate, as sedimentation has not kept up with sea level rise (Iglesias et al., 2008; Ramos et al., 2014b). Galician rias are classified according to their tectonic predetermination and geography into Higher, Lower and Cantabrian rias (e.g. Iglesias and Carballo, 2011). The Ribadeo ria belongs to the Cantabrian rias, in which the fluvial component is more important than the tectonic component. The Eo River feeds into the estuary with an annual mean discharge of $24\ m^3s^{-1}$ (Piedracoba et al., 2005). Although the Eo River affects the residual circulation of the estuary, tidal energy is the dominant forcing mechanism for the hydrodynamics (Piedracoba et al., 2005). The ria has undergone numerous modifications over the past century, including the Port of Ribadeo (west) and the Figueras port and shipyard (east) (Fig. 1). The Port of Ribadeo was significantly enlarged in 1991, effectively advancing the coastline eastward. This study investigates the effects of this enlargement on the sediment transport patterns, paying particular attention to the tidal delta and the inundation of the Eastern Channel. The Ribadeo ria provides stimulus to the local economy from its small industrial ports, commercial harbour, oyster farms and tourism. Past studies of the area have primarily been concerned with the hydro- and sedimentological characteristics of the estuary, as well as the effects of dredging and dumping (Asensio Amor and Gómez Miranda, 1984; Encinar and Rodríguez, 1983). Recently, the estuary has gained scientific interest as a potential candidate for tidal energy extraction (Ramos et al., 2014a, 2014b, 2013).

At present, the channels leading to ports in the Ribadeo estuary are dredged approximately every four years. In the case of Figueras, the launching of ships built at the shipyard necessitates frequent dredging along the eastern margin of the tidal delta. Movement of the delta is a subject of interest, due to its potential impact on the Eastern Channel and consequent effect on local dredging operations. Fig. 1 illustrates the location of the Ports of Ribadeo and Figueras, as well as the local bathymetric elevation.

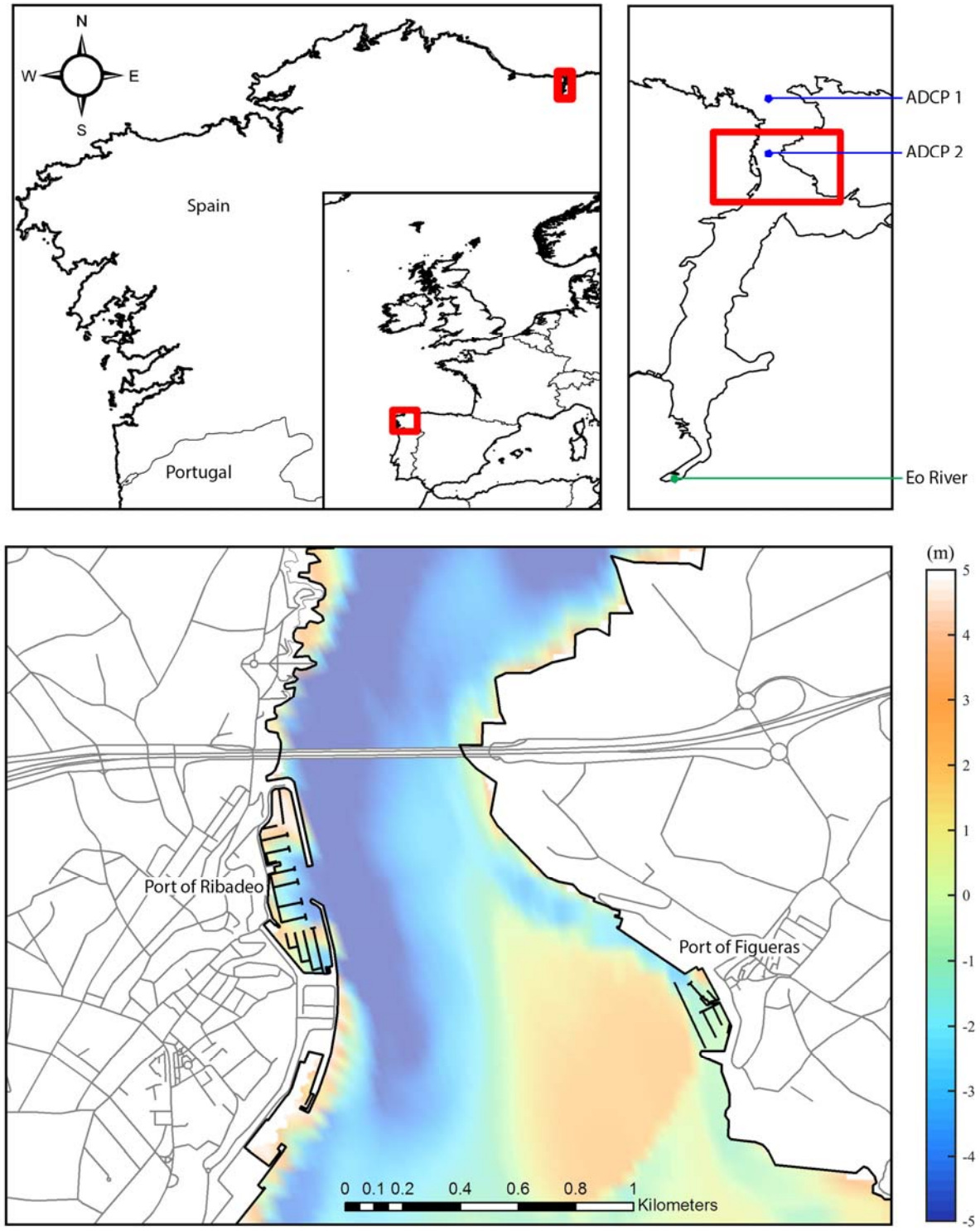

Fig. 1. Location map of Ribadeo estuary showing port developments, bathymetric features (elevation) and locations of Acoustic Doppler Current Profilers (ADCPs).

2. MATERIALS AND METHODS

This study undertakes process-based numerical modelling of 12 scenarios consisting of: 2 study cases; 2 tidal energy levels; and 3 morphological acceleration factors in order to analyse the morphodynamic response of the Ribadeo estuary to the port expansion. Section 2.1 outlines the data collected and adopted for the study, while Sections 2.2 and 2.3 describe the numerical model development and implementation, respectively.

2.1. DATA

A total of 35512 bathymetric sample points were digitised from multiple sources. The inner ria data were obtained from a bathymetry map of Ports Service of Principado de Asturias (2005), and the outer ria from a combination of nautical chart #4071 of the Spanish Hydrographic Institute and a 1:5000 cartography from the Galician Regional Government, Xunta de Galicia (Fig. 2). In order to investigate the morphodynamic response of the estuary to the development of the Port of Ribadeo, separate initial conditions were generated for pre- and post-construction scenarios, henceforth referred to as Case I and Case II respectively. The difference between the initial conditions in both cases pertain to the land formations (Fig. 2). Therefore the observed bed level variation between the two cases results from the expansion of the port. The pre-expansion scenario (Case I) was mapped to the historical land boundary, obtained from a 1944 cartography of the area supplied by the National Geographic Institute of Spain (2013).

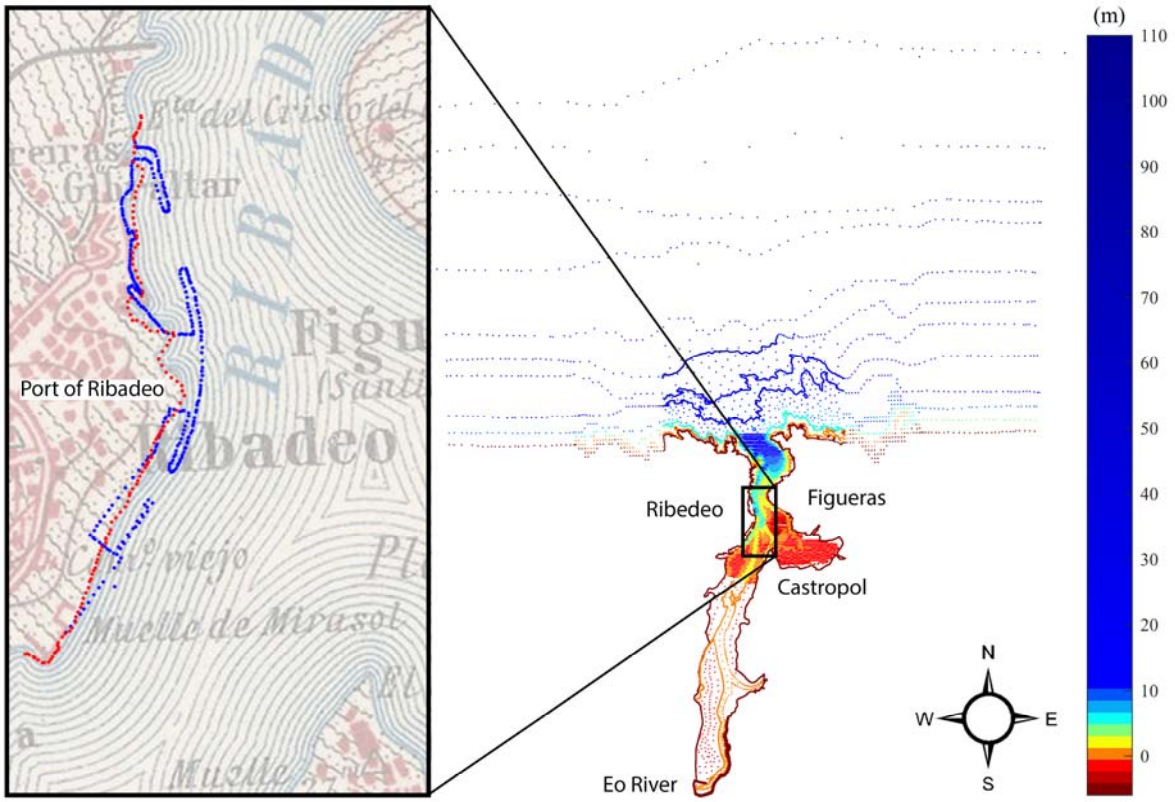

Fig. 2. Left: Comparison between Case I (•) and Case II (•) land boundaries. Right: Scatter plot of sample points adopted for bathymetric interpolation.

Tidal constituents were derived from the global ocean tide model TXPO 2.7 (Egbert et al., 1994), while Eo River daily influx data were obtained from CEDEX gauging station #1427 for the Spanish Ministry of Agriculture food and Environment (CEDEX, 2010). Following Ramos et al. (2014b), temperature and salinity at the ocean boundary were obtained from the Regional Ocean Modelling System (ROMS) (Otero et al., 2008). Spatially varying sediment data were adopted for the study, digitised from Encinar & Rodríguez (1983), with a median diameter range of 0.12×10^{-4} m $\leq d_{50} \leq 4.96 \times 10^{-4}$ m (Fig. 3).

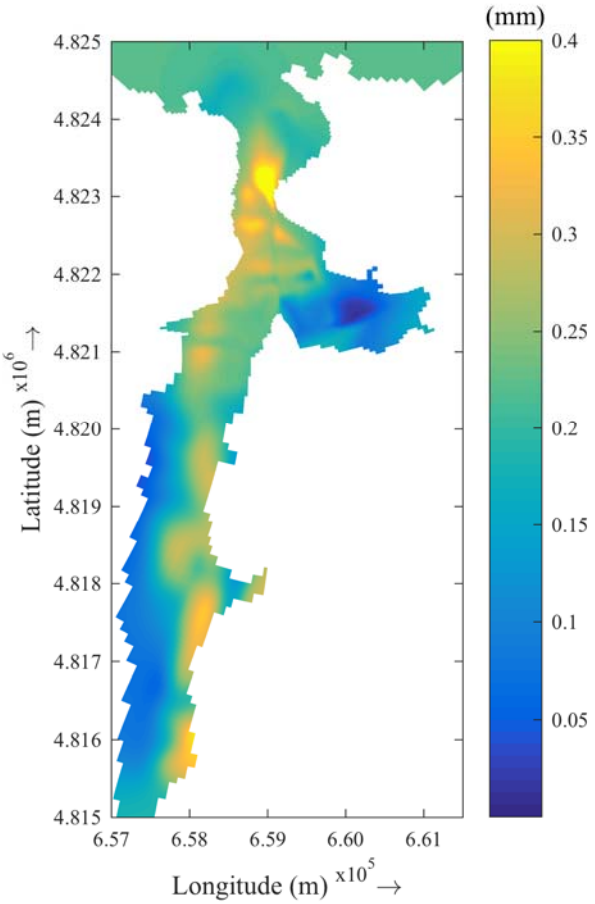

Fig. 3. Distribution of Median sediment diameter, d_{50} (mm), in Ria de Ribadeo

2.2. NUMERICAL MODEL

2.2.1. Hydrodynamics

A 2DH (depth-averaged) version of the process-based model Delft3D, was implemented for the investigation. Delft3D-FLOW is a finite difference code that solves the Navier-Stokes and transport equations under shallow-water and Boussinesq assumptions (Deltares, 2011). A brief description of the depth-averaged equations which govern the hydrodynamic model is presented below; further details can be found in Lesser et al. (2004).

Neglecting the effects of precipitation and evaporation, the continuity equation becomes

$$\frac{\partial \zeta}{\partial t} + \frac{\partial [h\bar{u}]}{\partial x} + \frac{\partial [h\bar{v}]}{\partial y} = 0\,, \qquad (1)$$

from which: $\bar{u}$ and $\bar{v}$, depth-averaged velocity in x and y directions (m s^{-1}), respectively; h, water depth (m); ζ , water level (m).

The depth-averaged horizontal momentum equations, assuming a quadratic friction law, null velocity and free slip (zero shear stress) boundary conditions at land boundaries, and neglecting Coriolis and wind effects, can be written

$$\left\{\begin{array}{l}\dfrac{\partial \bar{u}}{\partial t}+\bar{u}\dfrac{\partial \bar{u}}{\partial x}+\bar{v}\dfrac{\partial \bar{u}}{\partial y}+g\dfrac{\partial \zeta}{\partial x}+\dfrac{g\bar{u}\left|\sqrt{\bar{u}^2+\bar{v}^2}\right|}{C^2 h}-\nu\left(\dfrac{\partial^2 \bar{u}}{\partial x^2}+\dfrac{\partial^2 \bar{u}}{\partial y^2}\right)=0 \\ \dfrac{\partial \bar{v}}{\partial t}+\bar{v}\dfrac{\partial \bar{v}}{\partial y}+\bar{u}\dfrac{\partial \bar{v}}{\partial x}+g\dfrac{\partial \zeta}{\partial y}+\dfrac{g\bar{v}\left|\sqrt{\bar{u}^2+\bar{v}^2}\right|}{C^2 h}-\nu\left(\dfrac{\partial^2 \bar{v}}{\partial x^2}+\dfrac{\partial^2 \bar{v}}{\partial y^2}\right)=0\end{array}\right\}, \quad (2)$$

where: g, gravitational acceleration (m s^{-2}); ν, eddy viscosity (m^2 s^{-1}); and C, Chézy coefficient ($m^{1/2}$ s^{-1}). The Chézy coefficient is defined as

$$C = 18\log 12h/k_s\,, \quad (3)$$

where k_s is the Nikuradse roughness length-scale (e.g. Deltares, 2010).

The sand roughness scheme adopted, based on van Rijn (2007) , may be written

$$k_s = \min\left(\sqrt{k_{s,r}^2+k_{s,mr}^2+k_{s,d}^2}\,,\frac{h}{2}\right), \quad (4)$$

where $k_{s,r}, k_{s,mr}$ and $k_{s,d}$ denote the roughness of ripples, mega-ripples and dunes, respectively.

The depth averaged advection-diffusion equation, which is solved for salinity, temperature and sediment concentration may be written

$$\frac{\partial h\bar{c}}{\partial t}+\bar{u}\frac{\partial h\bar{c}}{\partial x}+\bar{v}\frac{\partial h\bar{c}}{\partial y}-D_h\left(\frac{\partial^2 h\bar{c}}{\partial x^2}+\frac{\partial^2 h\bar{c}}{\partial y^2}\right)+\lambda_d\bar{c}=S\,, \quad (5)$$

where $\bar{c}$ is the depth averaged concentration, D_h is the horizontal dispersion coefficient (m^2 s^{-1}), λ_d represents the first order decay process and S is the source term per unit area.

2.2.2. Sediment Transport

The sediment transport model implemented (Deltares, 2011) treats bed-load and suspended load sediment transport separately. A brief summary of the model equations will be included here; a detailed explanation is available in van Rijn et al. (2004). The transport formulation includes suspended load transport (S_{sus}) and bed load transport (S_b) to calculate the total transport (S_t),

$$S_t = S_{sus} + S_{bed}\,. \quad (6)$$

The suspended sediment transport is calculated with the advection-diffusion equation (Equation 5). The decay term is omitted and the source term per unit area (S) is calculated following van Rijn (1993) as

$$S = S_{sus} = c_a\bar{u}hF\,, \quad (7)$$

where S_{sus} denotes the suspended load transport rate (kg m^{-1} s), F is a dimensionless shape factor (van Rijn, 1984) and c_a is the reference concentration at height a above bed. The reference concentration is calculated as

$$c_a = f_{sus}\eta 0.015\rho_s \frac{d_{50}}{a}\frac{T_s^{1.5}}{D_*^{0.3}}, \quad (8)$$

from which: f_{sus}, calibration parameter; η, relative availability of sediment at seabed; ρ_s, sediment density (kg m^{-3}); d_{50}, median sediment grain size (m); D_*, dimensionless particle diameter; and T_s, dimensionless bed shear stress.

The bed load is calculated with the relation

$$|S_{bed}| = f_{bed}\eta 0.5\rho_s d_{50} u_*' D_*^{-0.3} T_s, \quad (9)$$

where S_{bed} is the bed load transport rate (kg m^{-1} s) and u_*' represents the effective bed shear velocity (m s^{-1}).

The effect of bed slope on sediment transport is included following Bagnold (1966). Hence, the bed slope effects are limited to the bed load component of the sediment transport.

2.2.3. *Morphodynamic Acceleration*

Variations in estuarine morphodynamics generally occur at a time scale several orders of magnitude greater than their hydrodynamic counterparts (Stive et al., 1990). A morphological acceleration factor (f_{MOR}) is adopted in response to this temporal disparity (Lesser et al., 2004; Roelvink, 2006). The method effectively extends the morphological time step, as the bed level changes calculated at each hydrodynamic time step ($\Delta t_{hydrodynamic}$) are magnified by the inclusion of a constant factor (Equation 10, Fig. 4).

$$\Delta t_{morphological} = f_{MOR}\,\Delta t_{hydrodynamic} \quad (10)$$

Historically, morphodynamic analyses were often prohibitively computationally taxing due to the number of hydrodynamic calculations required to obtain observable and meaningful morphological responses. Adopting a morphological acceleration factor (MORFAC) allows for high resolution, medium to long-term simulations to be carried out with minimal computational overheads (Dissanayake et al., 2009).

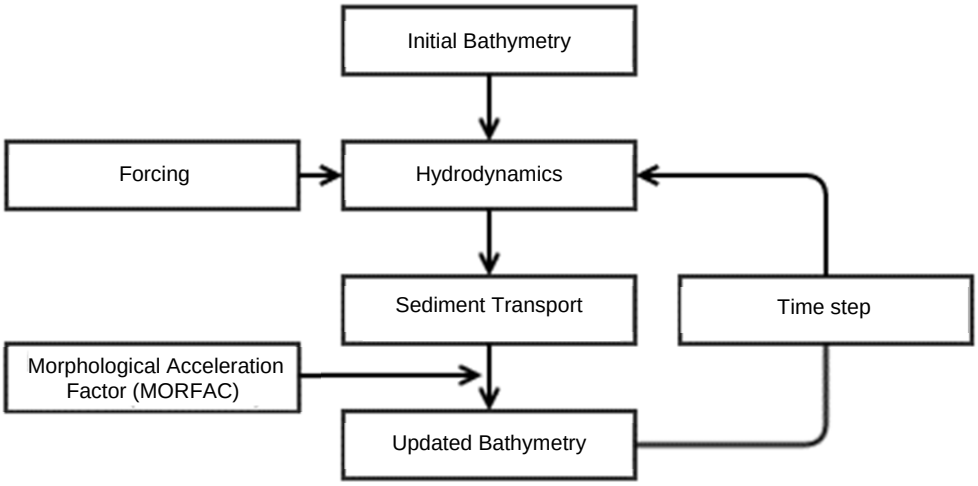

Fig. 4. Schematic diagram of adopted morphological model using MORFAC approach [adapted from Dissanayake et al. (2012)].

2.3. MODEL IMPLEMENTATION

2.3.1. Timeframe, Grid and Bathymetry

Models were run to simulate two 30-day periods, March 2010 (28/02/2010 00:00:00 – 30/03/2010 00:00:00) and June 2010 (31/05/2010 00:00:00 – 30/06/2010 00:00:00), corresponding to solstitial and equinoctial tides respectively, i.e. low and high tidal energy scenarios. Results from these two tidal energy scenarios were averaged to reduce seasonal influences on final bed levels. Seasonal variability is known to be of relevance in the Galician rias (Iglesias and Carballo, 2009). In each simulation a spin-up period of 7 days was implemented to guarantee that the initial hydrodynamic condition ("cold-start") does not affect the results in the period of interest. A time step of 9 seconds was adopted to ensure numerical stability.

Following Ramos et al. (2014b), the model utilised an Arakawa C-Grid, whereby water levels are prescribed at the centre of a grid cell, and velocities at the grid face mid-point. The model grid was curvilinear and spatially varying, focusing resolution on the ria, approaching 10 m × 25 m. From the ria, grid size increased in all directions to a maximum of approximately 400 m × 200 m at the ocean boundary (Fig. 5).

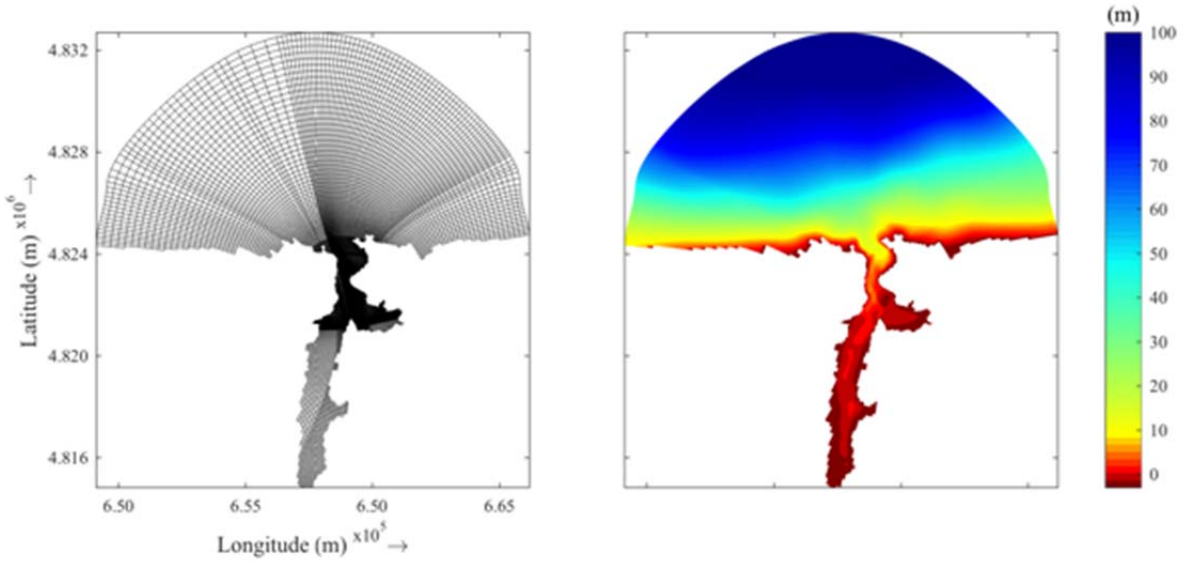

Fig. 5. Left: Computational Grid. Right: Interpolated bathymetry of Ribadeo area.

2.3.2. Boundary Conditions

The Ribadeo ria is a predominantly tidal forced estuary (Piedracoba et al., 2005) (Section 2). As such, an astronomically forced water level condition was imposed along the ocean boundary, including the nine major tidal harmonics to accurately represent the tidal asymmetry of the area (Ramos et al., 2013) (Table 1).

Table 1. Tidal constituents at water level boundary.

Constituent	Amplitude (m)	Phase (°)
M2	1.2513	91.40
S2	0.4396	122.17
M4	0.0169	311.70
MS4	0.0063	337.16
N2	0.2647	71.45
K2	0.1227	120.23
K1	0.0714	73.27
O1	0.0623	324.20
P1	0.0216	64.82

Daily averaged riverine influx was also included in model forcing, with a range of $6.235\ m^3s^{-1} \leq Q \leq 373.169\ m^3s^{-1}$. Temperature and salinity prescribed at the ocean boundary as 15.635 ℃ and 35.635 ppt respectively.

2.3.3. Morphology

To ensure robustness and identify progressive trends in the erosion/accretion process, the study adopted various MORFAC values: $f_{MOR} = 12;\ 24;\ 48$. Hence, each hydrodynamic month was equivalent to $1, 2$ or 4 years respectively. Results from MORFAC cases are denoted by t_n, where n corresponds to the number of morphological years associated with each scenario.

Though a definitive method for determination of critical MORFAC is not yet agreed upon (Ranasinghe et al., 2011), the adopted range is conservative in comparison with literature. Tidal forced models have adopted MORFAC values of several hundred to simulate morphological variation with centennial time scales. (Dissanayake et al., 2009; van der Wegen and Roelvink, 2008).

2.3.4. Initial Conditions

The breakwaters of the Port of Ribadeo were treated as boundaries prohibiting flow between computational cells (Deltares, 2011). Minor bathymetric variations between Cases I and II arise due to the interpolation and smoothing procedures applied to the sample data (Fig. 6). It is noted that these differences are almost entirely localised to the area of the harbour in the west. From this, it is assumed that any inter-case variation in final bed levels can be attributed to the harbour construction and its effects on estuarine hydro- and morphodynamics. For the sake of simplicity, the differences between Cases I and II are denoted by

$$\Delta a = a_{\text{Case II}} - a_{\text{Case I}}, \tag{11}$$

where a is a generic variable.

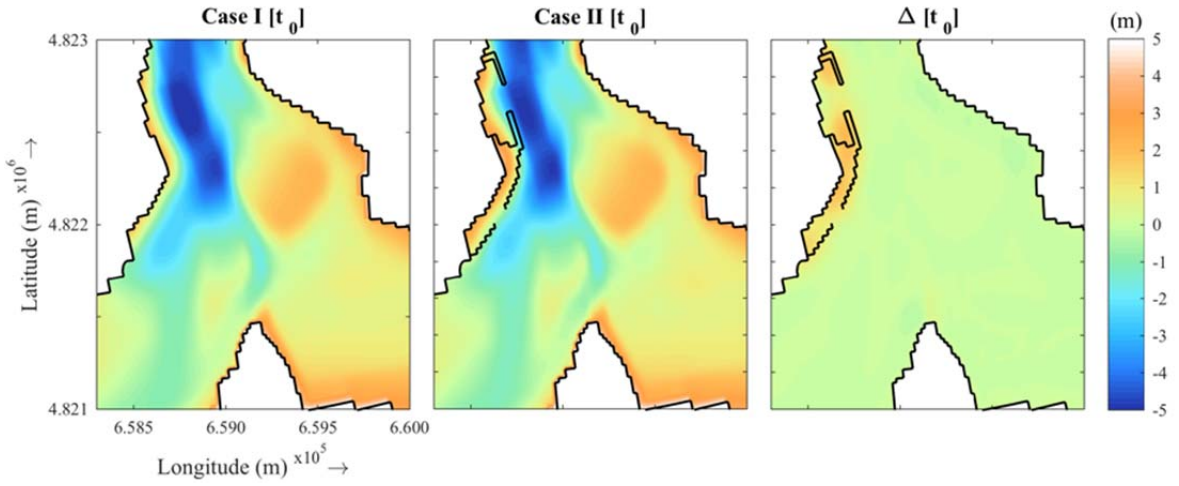

Fig. 6. Initial [t_0] model bathymetries and port implementation.

3. RESULTS AND DISCUSSION

3.1. VALIDATION

The hydrodynamic accuracy of the model was validated with data from two locations. The validation period spanned from 16th October to 5th November 2010. Two Acoustic Doppler Current Profilers (ADCPs) were deployed in the estuary, recording water level and current with a temporal resolution of 30 minutes. The first of the Sontek Argonaut-XR ADCPs (ADCP 1) was positioned towards the mouth of the ria, while ADCP 2 was located in the vicinity of the port (Fig. 1). Excellent agreement ($R > 0.95$) was found between simulated hydrodynamics and measured water level and flow velocities, northward and eastward, over the validation period for both ADCPs (Fig.7, Fig. 8, Fig. 9, Table 2). It may be concluded that the model accurately represented the hydrodynamics of the ria throughout the validation period.

Table 2. Correlation coefficient ($\boldsymbol{R}$) and Mean Squared Error ($\boldsymbol{MSE}$) for observed and computed water level ($\boldsymbol{\zeta}$) and eastward ($\boldsymbol{u}$) and northward ($\boldsymbol{v}$) velocities for ADCP 1 and 2.

	R_ζ	MSE_ζ (m)	R_u	MSE_u (m s^{-1})	R_v	MSE_v (m s^{-1})
ADCP 1	9.996×10^{-1}	3.107×10^{-4}	9.194×10^{-1}	5.936×10^{-3}	9.299×10^{-1}	4.787×10^{-3}
ADCP 2	9.999×10^{-1}	8.233×10^{-4}	9.513×10^{-1}	9.887×10^{-4}	9.777×10^{-1}	1.382×10^{-2}

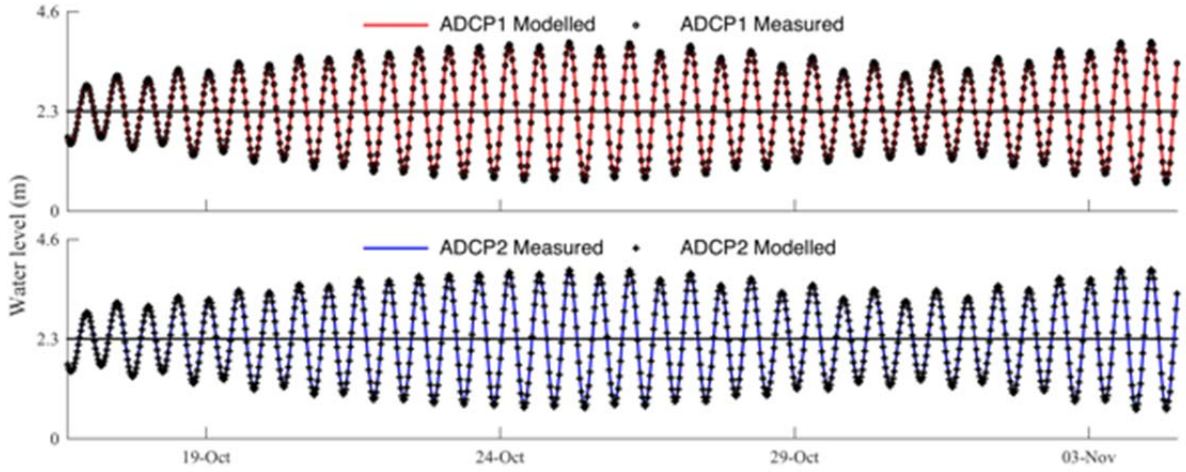

Fig. 7. Comparison of observed and computed time series for water level for ADCP1 and ADCP 2 over period of validation.

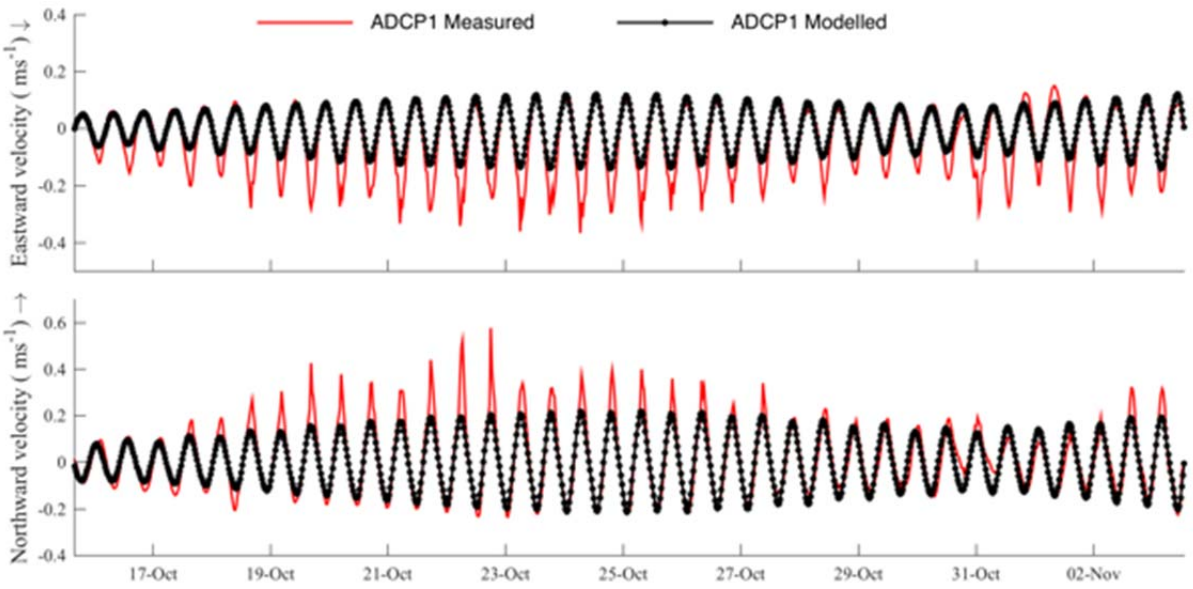

Fig. 8. Comparison of observed and computed time series for flow velocities at ADCP1 over period of validation.

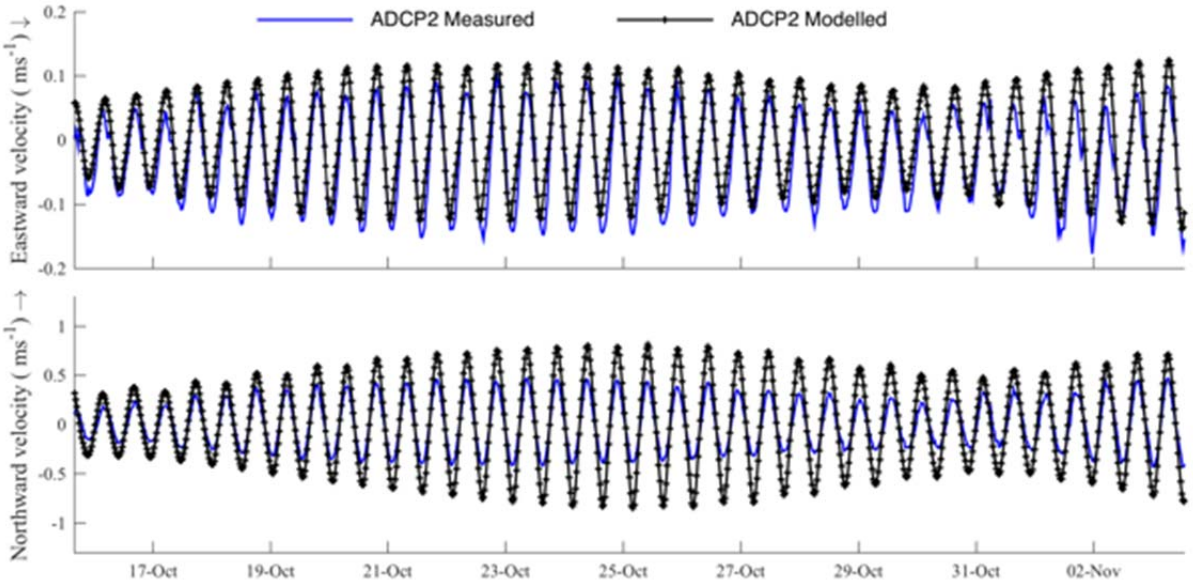

Fig. 9. Comparison of observed and computed time series for flow velocities at ADCP2 over period of validation.

3.2. MORPHODYNAMICS

3.2.1. Bathymetric Evolution

On initial inspection, several bathymetric evolution aspects of Case II are analogous to those of Case I, albeit with divergence in magnitude. Upon analysis, significant variations in spatial and temporal evolution trends of numerous bathymetric features are observable (Fig. 10).

At t_0, the primary channel splits into two smaller channels southward of the tidal delta. Both Case I and II illustrate a straightening of this channel with time, with a southward erosive trend. In Case II, the splitting of the channel is significantly reduced at t_1, evolving to form a dominant channel in the southwest with a small secondary channel, or tributary, in the southeast. At t_4, the tributary has been filled completely and the primary channel has taken a deeper, straighter, more efficient shape. Conversely, the secondary channel remains through bathymetric evolution of Case I, albeit with some morphological adjustment (Fig. 10).

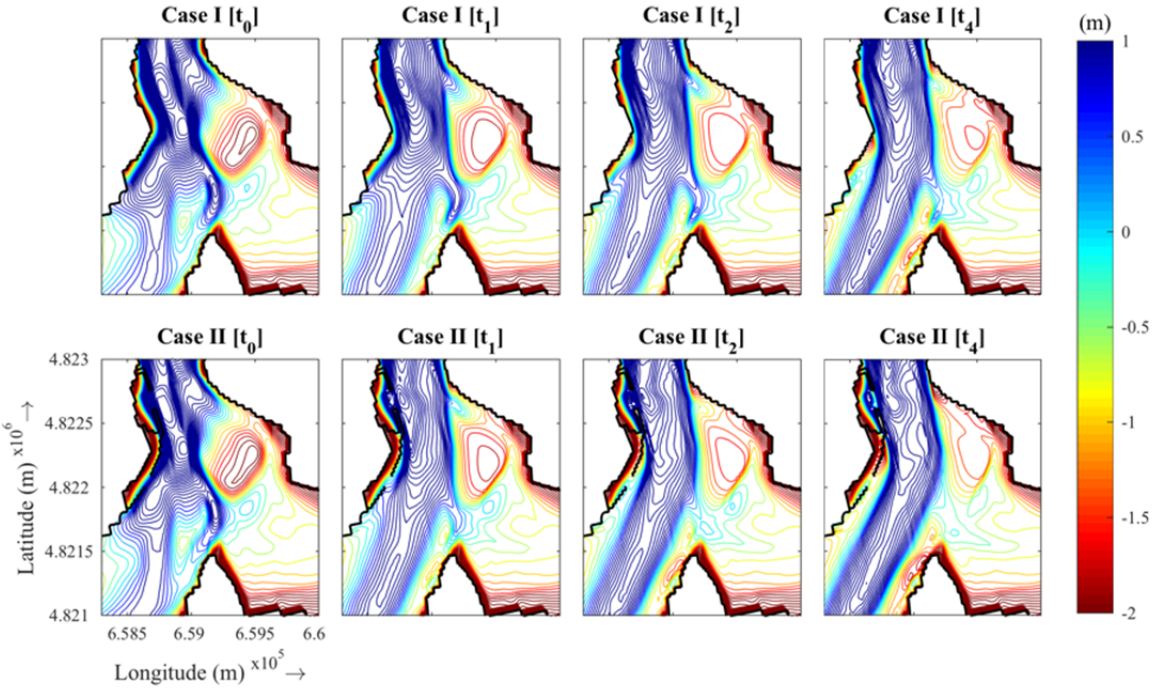

Fig. 10. Depth contour plot showing variation in primary channel response. Top: Case I (pre-development), Bottom: Case II (post-development), contour spacing of 0.2 m.

Variations in bathymetric evolution are observable in the area of the tidal delta (Fig. 11). Although the flattening of the delta is comparable, there is a distinction in its spatial evolution between Case I and II. In Case II, the tidal delta shifts eastward through time, as the eastern margin meets the land boundary and migrates northward, inundating the Eastern Channel. At t_4, the Eastern Channel is

completely inundated as the delta has become conjoined with the coastline. In Case I, the scale of inundation is significantly reduced. Although the eastward migration and associated channel infilling is apparent, the Eastern Channel remains present at t_4. The eastern margin of the delta also attaches to the coastline; however, the northward evolution of the attachment appears far slower than in Case II (Fig. 11).

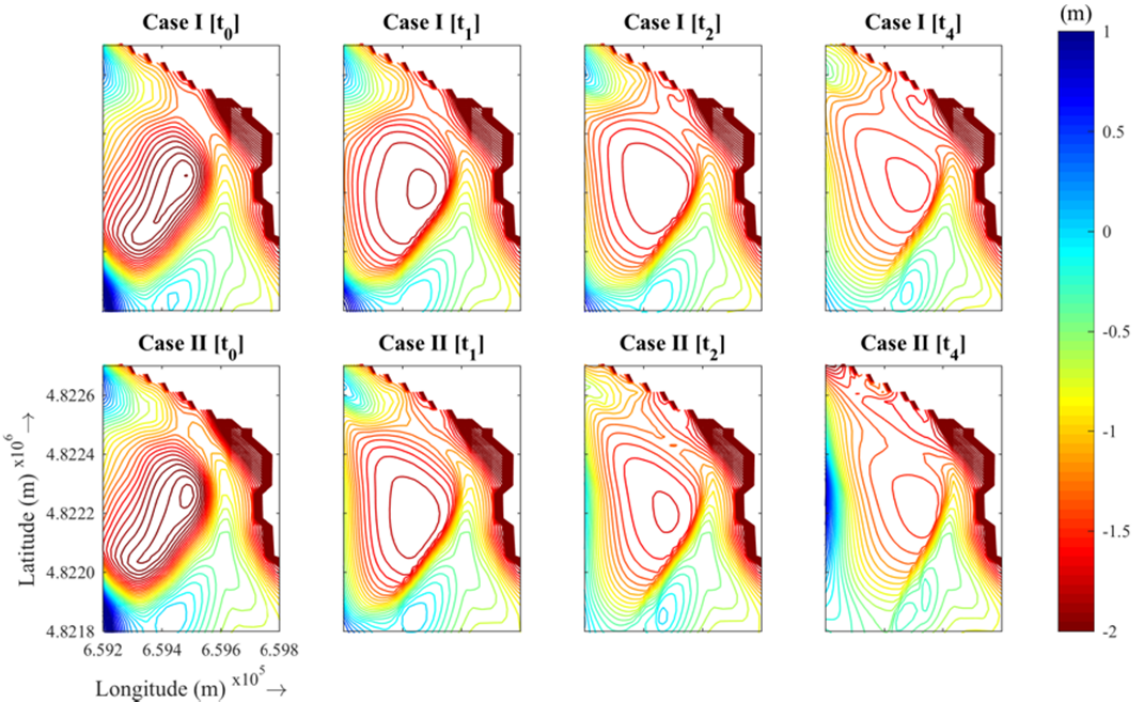

Fig. 11. Depth contour results, restricted to area of tidal delta, contour spacing of 0.1 m.

3.2.2. Bed level variation

Resulting bed level variations are calculated as

$$\Delta z = z_{tn} - z_{t0}, \tag{12}$$

where z represents bathymetric elevation (m).

The following analysis focuses on bed level variations beyond the local vicinity of the Port of Ribadeo, paying particular attention to the area of the tidal delta due to its effects on dredging operations in the Eastern Channel. The inter-case divergence of bathymetric responses is manifest in the vicinities of the primary channel and tidal delta (Fig. 12).

The erosive trends responsible for the primary channel deepening noted in Section 3.2.1 are clearly visible. These trends increase with time, as does the inter-case magnitude variation. At t_1, both Cases I and II show accretive trends through the centre of the primary channel, perpendicular to its orientation, bridging the sedimentation either side (Fig. 12 [A]). This sedimentation begins to weaken

in Case II, as the 'bridge' gives way to the primary flow, eventually becoming an erosive area at t_4. In contrast, the accretive trend strengthens with time in Case I.

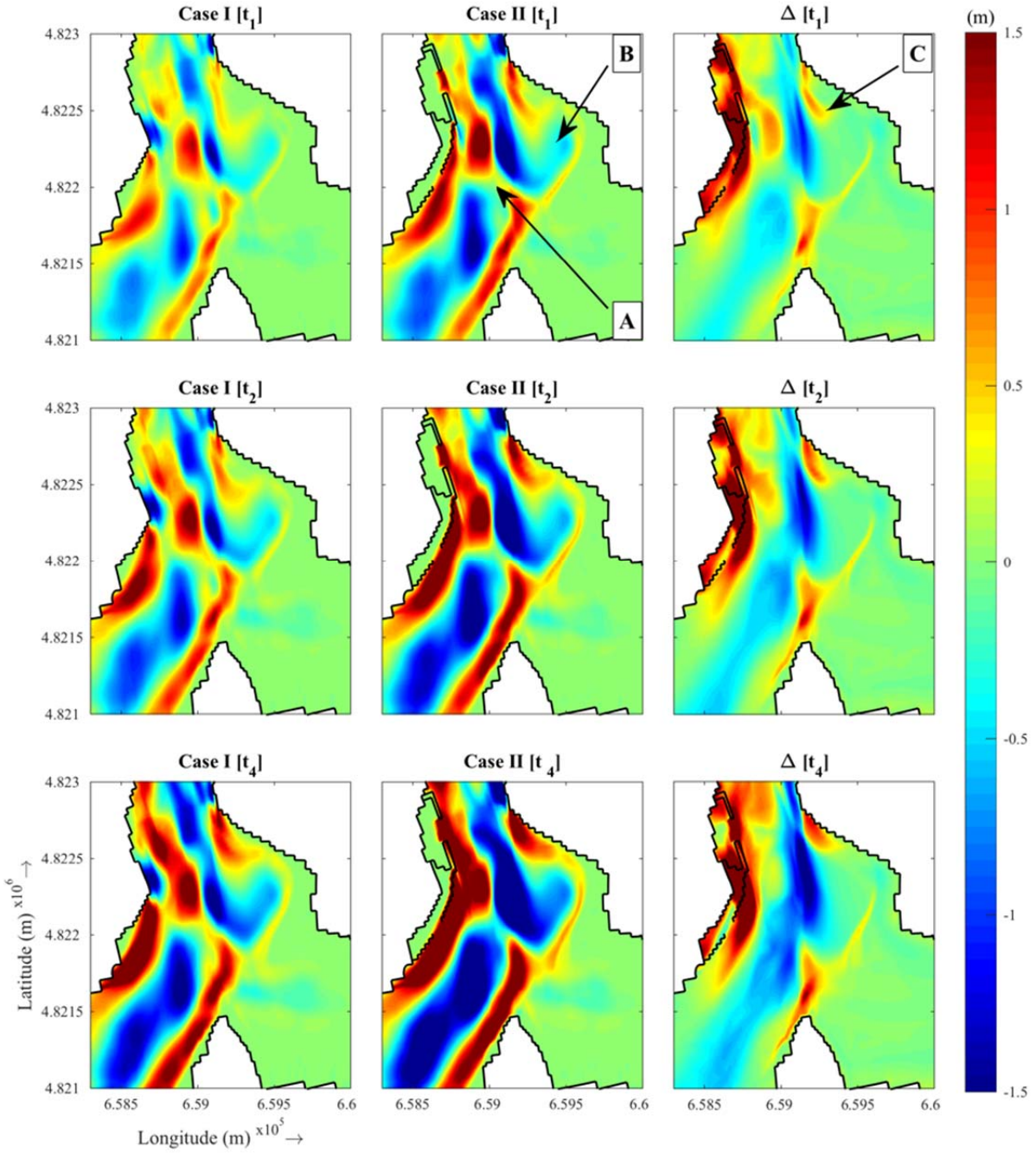

Fig. 12. Cumulative bed level variation (**Δz**). Left, Case I; Centre, Case II; Right, Inter-case variation.

Tidal delta flattening and eastward migration are clearly discernible in bed variation results (Fig. 12 [B]). The effective advancement of coastline caused by port development appears to have a significant effect on the tidal delta evolution, with Case II showing high levels of accretion in the north of the eastern delta margin. An inter-case divergence in delta migration and Eastern Channel sedimentation

is readily observable (Fig. 12 [C]). This accretive trend is critical as commercial operations in the area necessitate an open waterway, a requirement fulfilled with provision of dredging measures.

3.2.3. Cross-section

A profile investigation was carried out opposite the port development and through the area of the tidal delta and Eastern Channel to observe the morphodynamic responses noted in prior analyses (Fig. 13). The cross section investigation facilitates a more thorough analysis of bathymetric responses discussed in Sections 3.2.1 and 3.2.2, allowing identification and quantification of variation in several characteristic parameters. For the sake of simplicity, results are delineated into chainage zones denoted: Western $(0\ \text{m} > x \geq 150\ \text{m})$; Central $(150\ \text{m} > x \geq 330\ \text{m})$; Eastern $(330\ \text{m} > x \geq 660\ \text{m})$, where x corresponds to the easterly distance along the cross section A-A' (m).

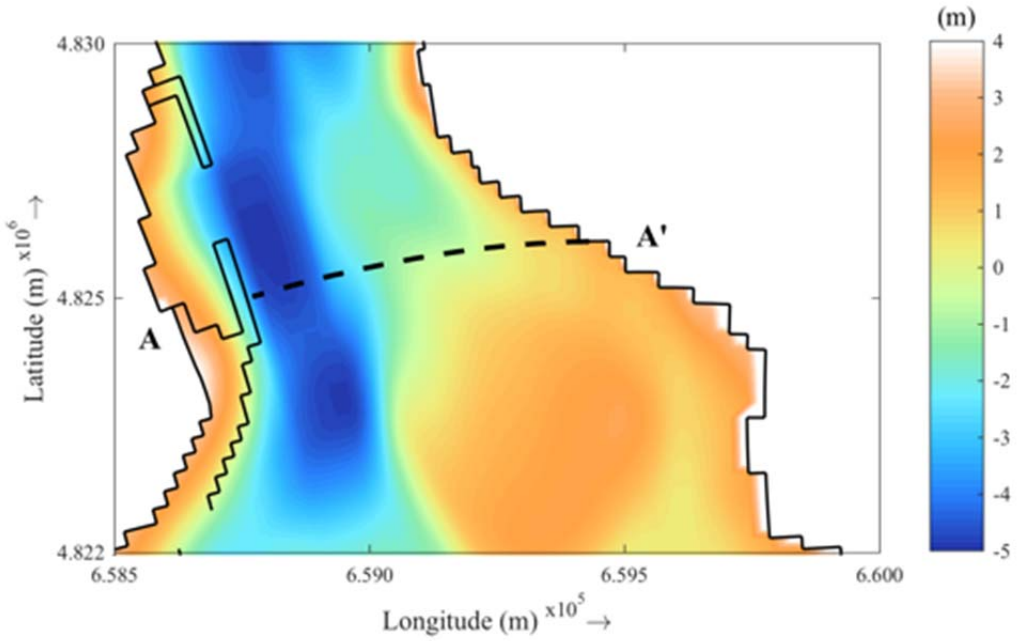

Fig. 13. Cross section A-A' (west-east) location on bathymetry (elevation).

The eastern point of inflexion between erosion and sedimentation, henceforth referred to as the critical point (x_c), shifts eastward by approximately 12 m/year in Case II. Comparatively, x_c is relatively stationary in Case I, varying less than 10 m between t_1 and t_4 (Fig. 13, Table 4).

Western accretion is greater in Case II than Case I, a result attributable to the simulated implementation of port development. The variation in Central erosive trends is clearly observable (Fig. 14). There are significant differences in the temporal evolution of this erosion, with peak erosion $(\min\ \Delta z)$ of Case II varying 0.615 m between t_1 and t_4, compared with 0.161 m for Case I (Fig. 10,

Table 3). Case I shows negligible Eastern accretion beyond $x = 420$ m at t_1 and t_2. At t_4, this accretive trend continues farther eastward, albeit with a significantly lower magnitude than that of Case II (Fig. 14). The inter-case increases in magnitude of Central erosion and Eastern accretion are clearly observable upon analysis of bed profile variation (Fig 15, Table 4).

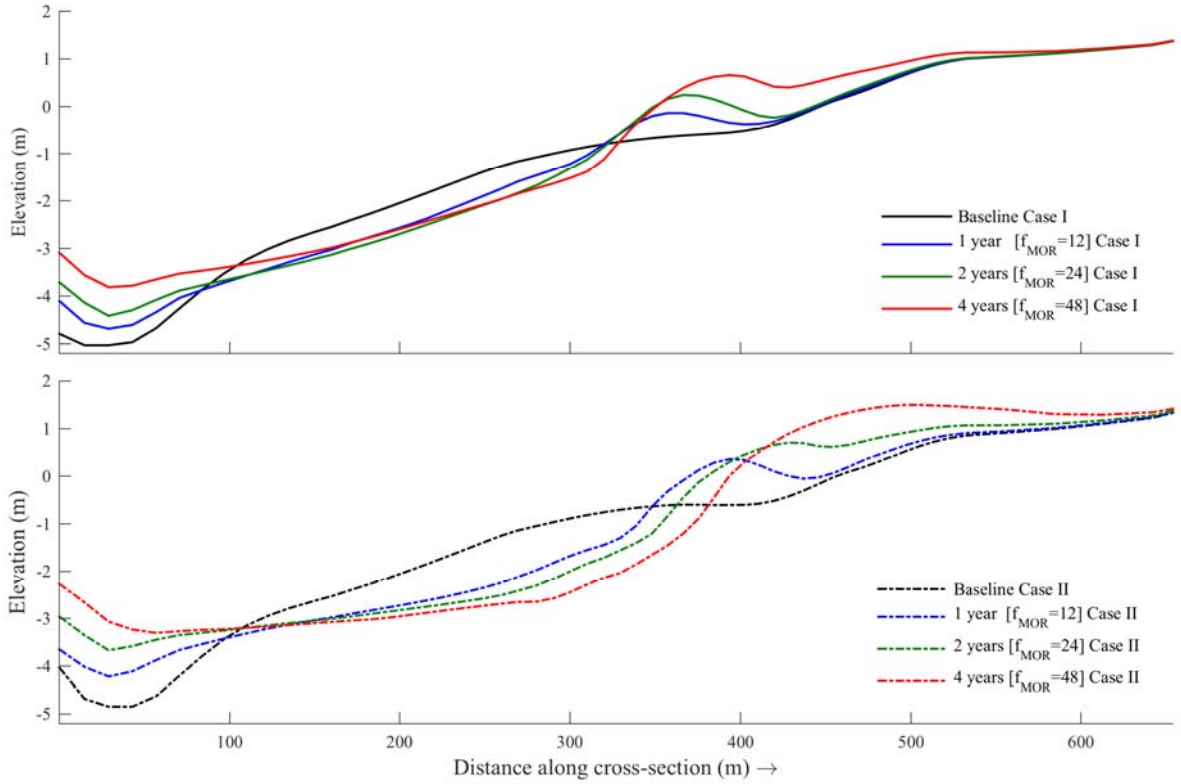

Fig. 14. Elevation profiles along Section A-A'. Top: Case I (–). Bottom: Case II (- -).

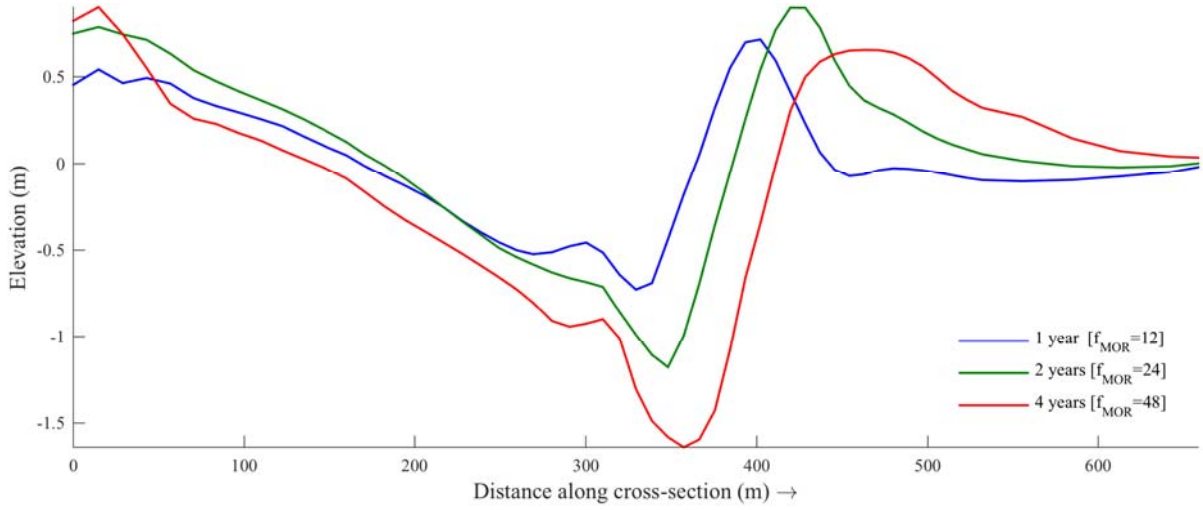

Fig. 15. Difference in resulting bed levels of Case I and II (**Δ**). Section A-A'.

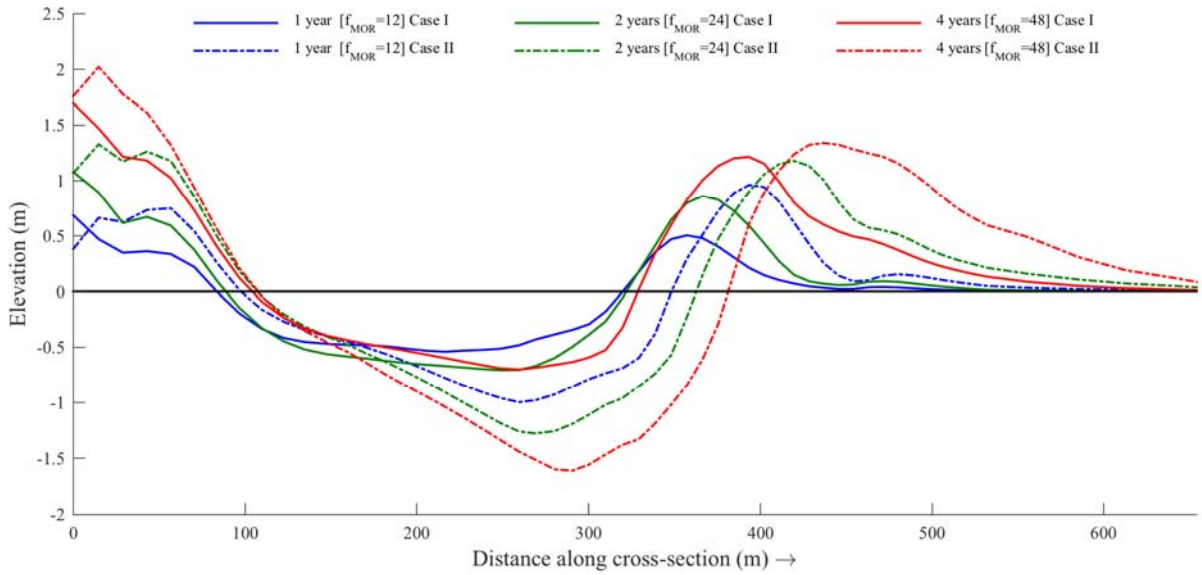

Fig. 16. Cumulative bed level variation (**Δz**) comparison of Case I (–) and Case II (- -). Section A-A'.

Bed level variation profiles from both study cases and all morphological acceleration factors are compiled in Fig. 16. Inclusion of an anthropogenic obstacle representing the Port of Ribadeo in simulations triggers increased magnitudes of Δz extrema in all areas of the profile: Western, Central and Eastern (Fig. 16, Table 3). Furthermore, Case II shows an increased lateral displacement of both the critical point (x_c) and location of Eastern peak accretion, as well as increased sedimentation unit volume at $x \geq x_c$ (Table 4).

Table 3. Bed level variation (**Δz**) extrema.

Time (years)	Western extreme (m)			Central extreme (m)			Eastern extreme (m)		
	Case I	Case II	Δ	Case I	Case II	Δ	Case I	Case II	Δ
1	0.686	0.750	0.064	-0.538	-0.997	-0.459	0.505	0.962	0.457
2	1.080	1.331	0.251	-0.706	-1.276	-0.570	0.860	1.180	0.320
4	1.697	2.022	0.325	-0.699	-1.612	-0.913	1.215	1.342	0.127

Table 4. Sedimentation cross section characteristics between study cases in tidal delta area.

Time (years)	Critical point ($x = x_c$) location (m)			Location of maximum Eastern accretion (m)			Sedimentation unit volume at $x \geq x_c$ (m^3/m)		
	Case I	Case II	Δ	Case I	Case II	Δ	Case I	Case II	Δ
1	320.0	348.3	28.3	357.6	393.6	36.0	32.1	69.3	37.2
2	320.0	366.7	46.7	366.7	419.8	53.1	60.4	120.9	60.5

4	329.6	384.7	55.1	393.6	437.1	43.5	129.8	183.2	53.4

The observed increases in all parameters shown in Tables 3 and 4 illustrate the effects of anthropogenic modification on estuarine morphodynamics. The results show a significant increase in eastward tidal delta evolution and associated Eastern Channel inundation caused by the Port of Ribadeo development, a detrimental outcome for local commercial operations.

3.2.4. Discussion

This work is focused on a particular estuary, and in particular on the effects of port expansion on the morphodynamics. These morphodynamic effects, alongside the hydrodynamic effects from which they stem directly, may cause ecological impacts that warrant examination. The increase in the shipping traffic can also have consequences for the ecology of the estuary. If ships anchor in the estuary, as is often the case, estuarine seagrass ecosystems may be affected. In the case of estuaries in which aquaculture or fishing are important, these activities may also be affected. In other words, port expansion in an estuary has potentially many environmental impacts which go beyond the morphodynamic effects with which this work is concerned – and all of which need addressing.

The presented modelling approach was adopted to limit the variation between study cases to the port expansion alone. Wind and wave forcing were neglected as they are not appropriate for morphological up-scaling which was applied in this study. In reality, there are a number of factors which may influence the morphological outcomes, including variability in weather patterns and sea-level rise.

The inherently vast range of free parameters and variables responsible for sediment movement, combined with the deterministically chaotic nature of numerical models (Lorenz, 1972) brings quantitative results into question (Dissanayake et al., 2012a). As a result of this uncertainty, the aims of the study were to qualitatively investigate trends in morphodynamics due to anthropogenic modifications and quantify them within the limitations of current modelling techniques.

The inclusion of dredging operations in simulations may increase the significance of existing historical aerial photographic analyses in validating modelled morphodynamics. With this information, it is possible to experiment with the dredging operations, potentially optimising existing practise to reduce commercial overheads. Furthermore, the presented modelling method may be adapted to other geographic areas of varying hydro- and morphodynamic environments in order to determine its transferability. This would allow for comparative studies to be undertaken, potentially increasing our understanding of morphodynamic responses to anthropogenic estuarine modifications.

The observable morphodynamic responses to the Port of Ribadeo expansion highlight the need for informed coastal management to consider any potentially detrimental effects to other areas of the

estuary. While the eastward movement of the tidal delta has been a focus of the present study due to it's impact on the port of Figueras, it is possible that this morphodynamic shift may affect other estuarine activities such as oyster farming, fishing and recreation. Beyond these anthropological effects, the possible environmental impacts also require consideration. For example, accretion in areas of seagrass and wetland habitats may have detrimental effects on local ecosystems (Erftemeijer and Robin Lewis, 2006).

Morpodynamic responses represent only one of many potential impacts port developments may have on the local environment and economy, including air and water quality and sediment composition (Puig et al., 2014) as well as consequences to land use in the local hinterland (e.g. Felsenstein et al., 2014). For this reason, an integrated management approach is required to ensure consideration of all potential impacts.

The capability to model morphological responses to anthropogenic obstacles provides the potential to reduce both adverse environmental impacts, and costs of coastal and estuarine developments. Currently, numerical models of coastal and estuarine environments tend to serve analytical purposes, furthering understanding of existing processes. With increases in accuracy and robustness, the models may find use in the design phase of coastal and estuarine developments. The benefits of understanding human interactions with estuarine morphodynamics may conceivably extend beyond sustainability, into the realms of advantageous design. For example, this knowledge may be used to design future defences, ports and harbours in such a way as to reduce dredging requirements, often a high on-going expense.

In order to make educated decisions about engineering solutions in estuarine environments, an understanding of all potential implications is required. Process based numerical models such as the present study have the capability to simulate an engineered solution and indicate the resulting changes in estuarine dynamics, allowing for informed coastal management. It is the authors opinion that future coastal and estuarine developments may require thorough morphological impact assessments to ensure all impacts are considered and to facilitate design optimisation.

4. CONCLUSIONS

The morphodynamic response of an estuary to the construction of port structures was investigated through a case study: the enlargement of the Port of Ribadeo. The investigation was carried out by means of numerical modelling, covering two study cases, representative of pre-development (Case I) and post-development (Case II) conditions. The tidal forced models accounted for daily influx from Eo River and spatially varying sediment size. Water levels and tidal currents were measured with two ADCPs, and excellent agreement was found between simulated and observed hydrodynamics. The

response to estuarine modification was investigated by means of morphological acceleration factors, corresponding to morphological times of 1, 2 and 4 years, in order to analyse temporal variations in resulting bathymetries.

Through investigation of final bed levels, cumulative erosion/sedimentation and bed profiles, several morphodynamic responses can be attributed to the modelled anthropogenic modification. The inter-case divergence in morphological results is manifest in accretive trends at the eastern tidal delta boundary and western port development, with an erosive trend in the primary channel. These differences between the two study cases represent the impact of the port expansion on the estuary.

Results indicate an increase in tidal delta migration and consequent infilling of the Eastern Channel arising from the development of the Port of Ribadeo. This result is critical due to the detrimental effect on commercial operations requiring passage through the Eastern Channel, necessitating increased dredging activity to keep up with the accelerated sedimentation. The results contribute to the understanding of morphodynamic responses, and consequently, the potential optimisation of coastal and estuarine management strategies.

ACKNOWLEDGEMENTS

A grateful thankyou is extended to Javier Abanades Tercero and José Victor Ramos Castro, who have provided guidance, and Germán Flor and Germán Flor-Blanco for their comments. Also, gracias to Port Service of Lugo and Port Service of Asturias for providing valuable data used in this study.

REFERENCES

Abanades, J., Greaves, D., Iglesias, G., 2015. Wave farm impact on beach modal state. Mar. Geol. 361, 126–135. doi:10.1016/j.margeo.2015.01.008

Abanades, J., Greaves, D., Iglesias, G., 2014a. Coastal defence through wave farms. Coast. Eng. 91, 299–307. doi:10.1016/j.coastaleng.2014.06.009

Abanades, J., Greaves, D., Iglesias, G., 2014b. Coastal defence using wave farms : The role of farm-to-coast distance. Renew. Energy 75, 572–582. doi:10.1016/j.renene.2014.10.048

Abanades, J., Greaves, D., Iglesias, G., 2014c. Wave farm impact on the beach profile: A case study. Coast. Eng. 86, 36–44. doi:10.1016/j.coastaleng.2014.01.008

Asensio Amor, I., Gómez Miranda, M.J., 1984. Oceanografía física: factores que condicionan la dinámica litoral en la ría del Eo, in: Cuadernos Da Área de Ciencias Mariñas. Seminario de Estudos Galego 1, pp. 79–90.

Bagnold, R.A., 1966. An approach to the sediment transport problem from general physics. US Geol. Surv. Prof. Pap., 422-I.

Buccino, M., Stagonas, D., Vicinanza, D., 2015. Development of a composite sea wall wave energy converter system. Renew. Energy 81, 509–522. doi:10.1016/j.renene.2015.03.010

Carballo, R., Iglesias, G., Castro, a., 2009. Residual circulation in the Ría de Muros (NW Spain): A 3D numerical model study. J. Mar. Syst. 75, 116–130. doi:10.1016/j.jmarsys.2008.08.004

Castillo-Manzano, J.I., González-Laxe, F., López-Valpuesta, L., 2013. Intermodal connections at Spanish ports and their role in capturing hinterland traffic. Ocean Coast. Manag. 86, 1–12. doi:10.1016/j.ocecoaman.2013.10.003

CEDEX, 2010. Estaciones de Aforo: Datos de estación foronómica [WWW Document]. Anu. Aforos 2010 - 2011. URL http://hercules.cedex.es/anuarioaforos/afo/estaf-datos.asp?indroea=1427 (accessed 7.25.14).

Dastgheib, A., Roelvink, J.A., Wang, Z.B., 2008. Long-term process-based morphological modeling of the Marsdiep Tidal Basin. Mar. Geol. 256, 90–100.

Deltares, 2011. Delft3D-FLOW. Simulation of multi-dimensional hydrodynamic flow and transport phenomena, including sediments – User Manual. Version 3.15, rev 14499.

Dissanayake, D.M.P.K., Ranasinghe, R., Roelvink, J.A., 2012a. The morphological response of large tidal inlet/basin systems to relative sea level rise. Clim. Change 113, 253–276.

Dissanayake, D.M.P.K., Roelvink, J.A., van der Wegen, M., 2009. Modelled channel patterns in a schematized tidal inlet. Coast. Eng. 56, 1069–1083.

Dissanayake, D.M.P.K., Wurpts, A., Miani, M., Knaack, H., Niemeyer, H.D., Roelvink, J.A., 2012b. Modelling morphodynamic response of a tidal basin to an anthropogenic effect: Ley Bay, East Frisian Wadden Sea – applying tidal forcing only and different sediment fractions. Coast. Eng. 67, 14–28.

Egbert, G.D., Bennett, A.F., Foreman, M.G.G., 1994. TOPEX/POSEIDON tides estimated using a global inverse model. J. Geophys. Res. 99, 24821.

Encinar, M. V., Rodríguez, G.F., 1983. Aportaciones para el conocimiento de la dinámica y sedimentación de la ria del Eo, Asturias-Galicia, NW de España. Cuadernos del CRINAS. Consejería de Agricultura y Pesca del Principado de Asturia.

Erftemeijer, P.L.A., Robin Lewis, R.R., 2006. Environmental impacts of dredging on seagrasses: A review. Mar. Pollut. Bull. 52, 1553–1572. doi:10.1016/j.marpolbul.2006.09.006

European Commission, 2011. Guidelines on the Implementation of the Birds and Habitats Directives in Estuaries and Coastal Zones with particular attention to port development and dredging. doi:10.2779/44024

Felsenstein, D., Lichter, M., Ashbel, E., 2014. Coastal congestion: Simulating port expansion and land use change under zero-sum conditions. Ocean Coast. Manag. 101, 89–101. doi:10.1016/j.ocecoaman.2014.08.001

Iglesias, G., Carballo, R., 2011. Can the Seasonality of a Small River Affect a Large Tide-Dominated Estuary? The Case of Ría de Viveiro, Spain. J. Coast. Res. 27, 1170–1182. doi:http://dx.doi.org/10.2112/JCOASTRES-D-11-00021.1

Iglesias, G., Carballo, R., 2009. Seasonality of the circulation in the Ría de Muros (NW Spain). J. Mar. Syst. 78, 94–108. doi:10.1016/j.jmarsys.2009.04.002

Iglesias, G., Carballo, R., Castro, A., 2008. Baroclinic modelling and analysis of tide- and wind-induced circulation in the Ría de Muros (NW Spain). J. Mar. Syst. 74, 475–484.

Kamphuis, J.W., 2006. Coastal engineering—quo vadis? Coast. Eng. 53, 133–140.

Kim, J., Park, J., 2015. Ocean & Coastal Management Mathematical modeling of coastal marine environments using observational data for coastal management. Ocean Coast. Manag. 116, 396–403. doi:10.1016/j.ocecoaman.2015.08.007

Kuang, C., Liu, X., Gu, J., Guo, Y., Huang, S., Liu, S., Yu, W., Huang, J., Sun, B., 2013. Numerical prediction of medium-term tidal flat evolution in the Yangtze Estuary: Impacts of the Three Gorges project. Cont. Shelf Res. 52, 12–26. doi:10.1016/j.csr.2012.10.006

Lesser, G.R., Roelvink, J. a., van Kester, J. a. T.M., Stelling, G.S., 2004. Development and validation of a three-dimensional morphological model. Coast. Eng. 51, 883–915.

Liu, C., 2013. NOAA Optimum Interpolation 1/4 Degree Daily Sea Surface Temperature Analysis [WWW Document]. Natl. Clim. Data Cent. - NOAA. URL http://www.ncdc.noaa.gov/sst/ (accessed 2.4.14).

López-Ruiz, A., Ortega-Sánchez, M., Baquerizo, A., Losada, M.A., 2012. Short and medium-term evolution of shoreline undulations on curvilinear coasts. Geomorphology 159-160, 189–200. doi:10.1016/j.geomorph.2012.03.026

Lorenz, E.N., 1972. Predictability: Does the flap of a butterfly's wings in Brazil set off a tornado in Texas?, in: American Association for the Advancement of Science Annual Meeting Prog. p. 139.

Maren, D.S. Van, Kessel, T. Van, Cronin, K., Sittoni, L., 2015. The impact of channel deepening and

dredging on estuarine sediment concentration. Cont. Shelf Res. 95, 1–14. doi:10.1016/j.csr.2014.12.010

Monge-Ganuzas, M., Cearreta, A., Evans, G., 2013. Morphodynamic consequences of dredging and dumping activities along the lower Oka estuary (Urdaibai Biosphere Reserve, southeastern Bay of Biscay, Spain). Ocean Coast. Manag. 77, 40–49.

Nacíonal Instituto Geográfico, 2013. Centro de Descargas [WWW Document]. Cent. Natl. Inf. Geográfica. URL http://centrodedescargas.cnig.es/CentroDescargas/buscar.do (accessed 8.10.14).

Ortega-Sánchez, M., Losada, M. a., Baquerizo, A., 2003. On the development of large-scale cuspate features on a semi-reflective beach: Carchuna beach, Southern Spain. Mar. Geol. 198, 209–223. doi:10.1016/S0025-3227(03)00126-9

Otero, P., Ruiz-Villarreal, M., Peliz, A., 2008. Variability of river plumes off Northwest Iberia in response to wind events. J. Mar. Syst. 72, 238–255.

Piedracoba, S., Souto, C., Gilcoto, M., Pardo, P.C., 2005. Hydrography and dynamics of the Ría de Ribadeo (NW Spain), a wave driven estuary. Estuar. Coast. Shelf Sci. 65, 726–738.

Puig, M., Wooldridge, C., Darbra, R.M., 2014. Identification and selection of Environmental Performance Indicators for sustainable port development. Mar. Pollut. Bull. 81, 124–130. doi:10.1016/j.marpolbul.2014.02.006

Ramos, V., Carballo, R., Álvarez, M., Sánchez, M., Iglesias, G., 2014a. A port towards energy self-sufficiency using tidal stream power. Energy 71, 432–444.

Ramos, V., Carballo, R., Álvarez, M., Sánchez, M., Iglesias, G., 2013. Assessment of the impacts of tidal stream energy through high-resolution numerical modeling. Energy 61, 541–554.

Ramos, V., Carballo, R., Sanchez, M., Veigas, M., Iglesias, G., 2014b. Tidal stream energy impacts on estuarine circulation. Energy Convers. Manag. 80, 137–149.

Ranasinghe, R., Swinkels, C., Luijendijk, A., Roelvink, D., Bosboom, J., Stive, M., Walstra, D., 2011. Morphodynamic upscaling with the MORFAC approach: Dependencies and sensitivities. Coast. Eng. 58, 806–811.

Roelvink, J. a., 2006. Coastal morphodynamic evolution techniques. Coast. Eng. 53, 277–287.

Sánchez, M., Carballo, R., Ramos, V., Iglesias, G., 2014. Tidal stream energy impact on the transient and residual flow in an estuary : A 3D analysis 116, 167–177. doi:10.1016/j.apenergy.2013.11.052

Saz-Salazar, S. del, García-Menéndez, L., Feo-Valero, M., 2012. Meeting the environmental challenge of port growth: A critical appraisal of the contingent valuation method and an application to Valencia Port, Spain. Ocean Coast. Manag. 59, 31–39. doi:10.1016/j.ocecoaman.2011.12.017

Spearman, J.R., Dearnaley, M.P., Dennis, J.M., 1998. A simulation of estuary response to training wall construction using a regime approach. Coast. Eng. 33, 71–89.

Stive, M.J.F., Roelvink, J.A., De Vriend, H.J., 1990. Large-scale coastal evolution concept, in: Proc. 22nd Int. Conf. on Coastal Engineering. ASCE, New York.

Taveira Pinto, F., 2004. The practice of coastal zone management in Portugal. J. Coast. Conserv. 10, 147. doi:10.1652/1400-0350(2004)010[0147:TPOCZM]2.0.CO;2

van der Wegen, M., 2010. Modeling morphodynamic evolution in alluvial estuaries. Ph.D Thesis. Delft University of Technology.

van der Wegen, M., Roelvink, J. a., 2008. Long-term morphodynamic evolution of a tidal embayment using a two-dimensional, process-based model. J. Geophys. Res. 113, C03016.

van Rijn, L.C., 2007. Unified View of Sediment Transport by Currents and Waves. I : Initiation of Motion, Bed Roughness, and Bed-Load Transport. J. Hydraul. Eng. 133, 649–667.

van Rijn, L.C., 1993. Principles of Sediment Transport in Rivers, Estuaries and Coastal Seas. Part I. AQUA Publications, The Netherlands.

van Rijn, L.C., 1984. Sediment transport, Part II: Suspended load transport. J. Hydraul. Eng. 110, 1613–1641.

van Rijn, L.C., Walstra, D.J.R., 2004. Description of TRANSPOR2004 and Implementation in Delft3D-ONLINE. WL| Delft Hydraul. Rep. Z3748.

Veloso-Gomes, F., Taveira-Pinto, F., 2003. Portuguese coastal zones and the new coastal management plans. J. Coast. Conserv. 9, 25. doi:10.1652/1400-0350(2003)009[0025:PCZATN]2.0.CO;2

Vicinanza, D., Contestabile, P., Quvang Harck Nørgaard, J., Lykke Andersen, T., 2014. Innovative rubble mound breakwaters for overtopping wave energy conversion. Coast. Eng. 88, 154–170. doi:10.1016/j.coastaleng.2014.02.004

Wu, C., Cai, F., Zhao, G., Zheng, Y., Lu, H., 2011. Impact of coastal engineering constructions on the topographic and morphological evolution of Quanzhou Bay, Fujian, China. Ocean Coast. Manag. 54, 544–555. doi:10.1016/j.ocecoaman.2011.04.002

Zhao, P., Bin, L.V., 2005. Port economy and its spatial effects: a case study on Rotterdam port, Netherlands [j]. Human Geography 5, 024.

FIGURE CAPTIONS

Fig. 1. Location map of Ribadeo estuary showing port developments, bathymetric features (elevation) and locations of ADCPs.

Fig. 2. Left: Comparison between Case I (•) and Case II (•) land boundaries. Right: Scatter plot of sample points adopted for bathymetric interpolation.

Fig. 3. Distribution of Median sediment diameter, d50 (mm), in Ria de Ribadeo

Fig. 4. Schematic diagram of adopted morphological model using MORFAC approach [adapted from Dissanayake et al. (2012)].

Fig. 5. Left: Computational Grid. Right: Interpolated bathymetry of Ribadeo area.

Fig. 6. Initial [t_0] model bathymetries and port implementation.

Fig. 7. Comparison of observed and computed time series for water level for ADCP1 and ADCP 2 over period of validation.

Fig. 8. Comparison of observed and computed time series for flow velocities at ADCP1 over period of validation.

Fig. 9. Comparison of observed and computed time series for flow velocities at ADCP2 over period of validation.

Fig. 10. Depth contour plot showing variation in primary channel response. Top: Case I (pre-development), Bottom: Case II (post-development), contour spacing of 0.2 m.

Fig. 11. Depth contour results, restricted to area of tidal delta, contour spacing of 0.1 m.

Fig. 12. Cumulative bed level variation (Δz). Left, Case I; Centre, Case II; Right, Inter-case variation.

Fig. 13. Cross section A-A' (west-east) location on bathymetry (elevation).

Fig. 14. Elevation profiles along Section A-A'. Top: Case I (-). Bottom: Case II (- -).

Fig. 15. Difference in resulting bed levels of Case I and II (Δ). Section A-A'.

Fig. 16. Cumulative bed level variation (Δz) comparison of Case I (-) and Case II (- -). Section A-A'.